Quantum thermal Hall effect in graphene

Wen Long,[1] Hui Zhang,[2] and Qing-feng Sun[2,*]
[1]*Department of Physics, Capital Normal University, Beijing 100048, China*
[2]*Institute of Physics, Chinese Academy of Sciences, Beijing 100190, China*
(Received 1 July 2011; published 5 August 2011)

The quantum thermal Hall effect in a six-terminal graphene device subjected to a thermal gradient and a perpendicular magnetic field is theoretically studied. We find that, when the Dirac-point energy is far away from the Fermi energy, the Hall thermal resistance has well-quantized plateaus and the longitudinal thermal resistance is zero at low temperature. On the other hand, when the Dirac-point energy is near the Fermi energy, a fine structure with a negative Hall-Lorentz number is exhibited in which the Wiedemann-Franz law is violated. This fine structure has a good scaling behavior and the analytical scaling functions are also obtained.

DOI: 10.1103/PhysRevB.84.075416 PACS number(s): 73.43.−f, 73.50.Lw, 72.80.Vp

I. INTRODUCTION

Since first discovered in 1879, the Hall-type effect[1–4] has always been a fascinating topic in condensed matter physics. It describes the phenomenon of a transverse bias induced by a longitudinal current. The Hall effect is the generation of transverse voltage from the longitudinal electric current in the presence of a magnetic field. Since then, a series of Hall related effects have been discovered including the quantum Hall effect (QHE),[1] spin Hall effect,[2] anomalous Hall effect,[3] quantum spin Hall effect,[4] etc., and many fascinating properties were revealed. Taking QHE as an example, the conductance is quantized with integer plateaus due to the Landau levels in the presence of a magnetic field.[1] Apart from the electric charge transport, the thermal transport has received more and more attention in recent years. Generally speaking, the thermal conductance and thermoelectric coefficient are more sensitive to details of device such as the density of states, etc.,[5,6] so they can provide more information such as the derivative of transmission coefficient with respect to energy. But in the early days, they were paid little attention to and even often neglected because of the experimental difficulties. With the development of microfabrication technology and low-temperature measurement technology, however, the thermal transport becomes feasible nowadays.[7–9] For instance, the Nernst effect, a Hall-type effect in which a transverse voltage is generated by a longitudinal thermal current, has been observed in many systems, including high-T_c superconductivity,[7] graphite,[8] etc., and the spin Seebeck effect[10] was also discovered recently.

In recent years, another research topic that has been extensively investigated is the graphene.[11] The graphene is an ideal two-dimensional material of monolayer hexagonal lattice of carbon atoms,[12] and has a unique linear dispersion of low-lying energy leading to many peculiar properties. For instance, its quasi-particles show a relativistic-like behavior and its Hall plateaus locate at the half-integer values.[11]

In this paper, we study the thermal Hall effect (THE) in graphene. Similar to the Hall effect, THE is the generation of transverse temperature difference resulting from a longitudinal thermal current.[13–17] In general, for the classical case, Wiedemann-Franz (WF) law is obeyed in which the ratio of thermal conductivity κ to electrical conductivity σ remains a constant: $L_{xy} = \kappa_{xy}/(\sigma_{xy}T) = \pi^2 k_B^2/(3e^2)(\equiv L_0)$, where T is absolute temperature, subscript $\{xy\}$ indicates the transverse direction, and L_{xy} is named Hall-Lorentz number. But in the quantum system or in the presence of various interactions, the WF law may not be held. Recently, THE and quantum THE (QTHE) have generated a great deal of interest, and have been widely studied within various systems including high-T_c superconductivity,[15] impurity-doped iron[16], doped graphene,[17] etc. In this paper, we consider a six-terminal graphene Hall bar subjected to a perpendicular magnetic field and a longitudinal thermal gradient [see the inset in Fig. 1(d)]. Due to the thermal gradient, a longitudinal thermal current flows through the device, in which high energy carriers flow from left to right while the low energy ones flow in the opposite direction. So, the high and low energy carriers are deflected toward the opposite transverse edges in this case, accordingly a transverse temperature difference is exhibited. The results clearly show that the QTHE emerges at low temperature and the Hall thermal resistance has quantized plateaus with the plateaus values being at half integer, which are robust against the disorder. Moreover, while the Dirac point is near the Fermi energy, both the Hall and longitudinal thermal resistances exhibit a fine structure with a negative Hall-Lorentz number.

The rest of this paper is organized as follows. In Sec. II, we describe the model and give the details of our calculation. In Sec. III, we show the numerical results of QTHE along with discussions. Finally, the conclusion is presented in Sec. IV.

II. MODEL AND METHOD

In the tight-binding representation, the six-terminal graphene device [see inset of Fig. 1(d)] can be described by the Hamiltonian:[18,19] $H = \sum_i \epsilon_i a_i^\dagger a_i - \sum_{\langle ij \rangle} t e^{i\phi_{ij}} a_i^\dagger a_j$, where $a_i^\dagger(a_i)$ denotes the creation (annihilation) operator at the site i and ϵ_i is the on-site energy (i.e., the energy of Dirac point). While in the absence of disorder, we set $\epsilon_i \equiv E_0$ for any site i. The second term in Hamiltonian describes the nearest neighbor hopping with t being the hopping energy. In the presence of magnetic field B, a phase ϕ_{ij} is added in the hopping term.[18,19] In the calculation, we used the zigzag edge graphene ribbon. We point that the results are the same for the armchair edge (see Fig. 4) and other chiral edges.

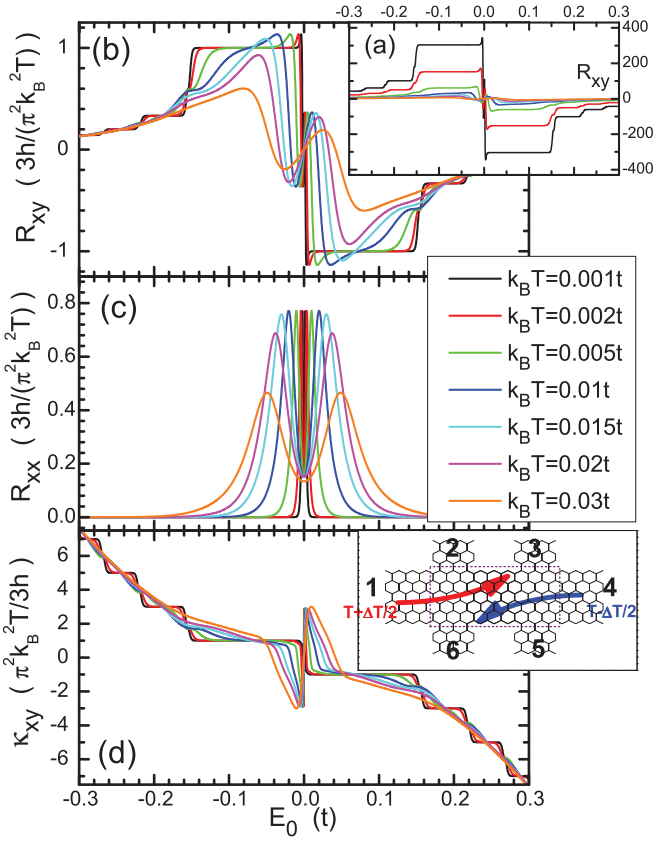

FIG. 1. (Color online) (a) is the Hall thermal resistance $R_{xy}(h/k_B)$ vs the Dirac-point energy E_0. (b)–(d), respectively, show the dimensionless thermal resistance R_{xy}, R_{xx}, and thermal conductance κ_{xy} vs E_0 at different temperatures. The parameters are $N = 50$, $L = 50$, $\phi = 0.007$, and the legend is for all panels. The inset of panel (d) is the schematic diagram for the six-terminal graphene device.

The heat flux flowing to the terminal n can be calculated from the Landauer-Büttiker-type formula:[20]

$$Q_n = (1/h)\sum_m \int (E - eV_n)T_{nm}(E)[f_n(E) - f_m(E)]dE, \tag{1}$$

where $T_{nm}(E)$ represents the transmission coefficient of electron from terminal m to terminal n at energy E, and it can be calculated through the equation $T_{nm}(E) = \mathbf{Tr}[\Gamma_n \mathbf{G}^r \Gamma_m \mathbf{G}^a]$, where $\Gamma_n(E) = i[\Sigma_n^r(E) - \Sigma_n^a(E)]$ and Green's function $\mathbf{G}^r(E) = [\mathbf{G}^a(E)]^\dagger = \{E\mathbf{I} - \mathbf{H}_C - \sum_n \Sigma_n^r\}^{-1}$. Here, $\mathbf{H}_C$ is the Hamiltonian of the central region [see the dotted box in inset of Fig. 1(d)] and $\Sigma_n^{r,a}$ is the self-energy due to the coupling of the terminal n. The size of central region is specified by the width N and length $2N + L$. In Fig. 1(d), the schematic diagram of graphene device has $N = 3$ and $L = 3$. Besides, $f_n(E) = 1/\{\exp[(E - eV_n)/k_B(T + T_n)] + 1\}$ is the Fermi distribution function in terminal n with chemical potential eV_n and temperature $(T + T_n)$. In the linear response regime, it can be expanded around the Fermi energy $E_F = 0$ and temperature T as

$$f_n(E) = f_0(E) - e\frac{\partial f_0}{\partial E}V_n + \frac{\partial f_0}{\partial T}T_n, \tag{2}$$

where $f_0 = 1/\{\exp[E/k_BT] + 1\}$ is the Fermi distribution under zero bias and zero thermal gradient. The charge current flowing to the terminal n can also be obtained from the Landauer-Büttiker formula:[21]

$$I_n = (e/h)\sum_m \int T_{nm}(E)[f_n(E) - f_m(E)]dE. \tag{3}$$

In our simulation, a thermal gradient ΔT is applied between terminals 1 and 4, so that $T_{1/4} = \pm\Delta T/2$, and a longitudinal thermal current flows via the chiral edge modes. The boundary conditions for the transverse terminals are $Q_n = 0$ ($n = 2, 3, 5, 6$) because they are the temperature probes. We assume there is no net charge current existing in the device, thus $I_n = 0$ ($n = 1, \ldots, 6$). Finally, by using Eqs. (1)–(3) combined with these boundary conditions, all thermal-gradient-induced voltages V_n and temperature T_n as well as longitudinal thermal current Q can be obtained. Specifically, the longitudinal and Hall thermal resistances are defined as $R_{xx} = (T_2 - T_3)/Q$ and $R_{xy} = (T_2 - T_6)/Q$ with $Q \equiv Q_1 = -Q_4$. Furthermore, the Hall thermal conductance reads $\kappa_{xy} = R_{xy}/(R_{xx}^2 + R_{xy}^2)$. In the following calculation, we use $t \approx 2.75$ eV as energy unit, and $3h/(\pi^2 k_B^2 T)$ as dimensionless thermal resistance unit. The size N and L are chosen to be $N = 50$ and $L = 50$ with the central region being approximately 21.2×37 nm^2. In fact, all results are insensitive to the size, except when it is very small. The magnetic field is represented by the parameter 2ϕ which is the magnetic flux in a honeycomb lattice.[18,19]

III. NUMERICAL RESULTS AND DISCUSSIONS

We first study the Hall and longitudinal thermal resistances, R_{xy} and R_{xx}, at different temperatures T. Three features are clearly revealed from Figs. 1(a) to 1(c). First, when $|E_0 - E_F| > 5k_BT$ at low temperatures, R_{xy} is well quantized exhibiting QTHE due to the Landau levels and chiral edge states. Second, when E_0 is near the Fermi energy $E_F = 0$, both R_{xy} and R_{xx} have fine structures which will be discussed in detail in the next paragraph. Third, with the increase of temperature, R_{xy} reduces monotonously and the quantized plateaus become smeared. The plateaus finally disappear when k_BT reaches room temperature (e.g., $k_BT = 0.01t$). This can be seen more clearly in Fig. 1(b) where R_{xy} is in the unit of $3h/(\pi^2 k_B^2 T)$ so that it is dimensionless. In the low temperature regime, due to the linear low-lying energy dispersion R_{xy} has quantized plateaus at half-integer values instead of integer values in the usual two-dimensional electron gas (2DEG).[13] In particular, at these plateaus the WF law is satisfied that $L_{xy} = L_0$,[14] because of the absence of backscattering. In the high temperature regime, however, the quantization characteristics vanishes and no plateaus can be observed any more. Besides, due to particle-hole symmetry, we have $R_{xy}(-E_0) = -R_{xy}(E_0)$ regardless of T, magnetic flux ϕ, and the device size. For the longitudinal thermal resistance R_{xx}, on the other hand, the symmetry becomes even, i.e., $R_{xx}(E_0) = R_{xx}(-E_0)$. From Fig. 1(c), we see that R_{xx} exhibits a symmetric double peak structure and $R_{xx} \neq 0$ at $E_0 = 0$. At low temperatures, the sharp peak is located in the vicinity of $E_0 = 0$. It becomes broadened with the peak position shifted away from $E_0 = 0$ as temperature increases. The peak value is a constant up to $k_BT = 0.01t$

(corresponding to room temperature). Upon further increasing the temperature, the peak value starts to decrease. Next, let us examine the behavior of Hall thermal conductance κ_{xy} at different temperatures [see Fig. 1(d)]. Similar to R_{xy}, at low T, κ_{xy} also exhibits quantized plateau that is eventually destroyed as the temperature approaching to room temperature. We note that although the quantized plateaus disappear, the values of κ_{xy} do not change much indicating the fact that the THE still exists although QTHE has been completely destroyed. Furthermore, in the high T regime, we have the asymptotic behavior $\kappa_{xy} \propto E_0^2$. This is because the thermal conductance is sensitive to the occupied particle number n and for graphene we have $n \propto E_0^2$ due to linear low-lying energy dispersion.

Let us further examine the fine structure of the Hall and longitudinal resistances in detail. For this purpose, we zoom in Figs. 1(b) and 1(c) and plot them in Figs. 2(a) and 2(b), respectively. We can see clearly that R_{xy} does not drop monotonously from 1 to -1 when E_0 passes through $E_F = 0$ with the carriers changing from the electrons to holes. Specifically, with the increase of E_0, R_{xy} first increases and then drops after reaching a maximum value. It then quickly drops to a negative value in the region $E_0 < 0$. Finally, R_{xy} increases again and reaches $R_{xy} = 0$ at $E_0 = 0$. For $E_0 > 0$, the behavior of R_{xy} obeys the relation $R_{xy}(-E_0) = -R_{xy}(E_0)$. In particular, R_{xy} is positive in the vicinity of origin. Within this regime, the WF law is clearly violated with its Hall-Lorentz number $L_{xy} < 0$. Here, the negative L_{xy} originates from the electron- and hole-like edge states propagating in opposite directions,[14] and the unique zeroth Landau level which has both electron- and hole-like behaviors. This feature shows essential difference in comparison with the usual 2DEG, in which L_{xy} is always positive,[13] even if the system has both electron and hole. This fine structure indicates that non-interaction graphene resembles the interaction two-dimensional electron gas in the fractional quantum Hall regime. For R_{xx}, as seen in Fig. 2(b), two peaks emerge regardless of temperature. This double peak structure seems to be analogous to that in the disorder 2DEG.[13] But now the double peak structure can survive in the clean graphene device due to the upstream propagating electron- and hole-like edge states. Of more importance, R_{xx} still has non-zero value even at $E_0 = 0$ in which the density of state is actually 0.

In the following, we shall give detailed explanation of such negative Hall-Lorentz number. At first, let us consider the region of $E_0 < 0$ with E_0 is very close to 0. In this region, at the finite temperature, the system has both electron- and hole-like carriers with the filling factor ν_e of electron-like carriers larger than that of hole-like carriers ν_h. Although the electron- and hole-like carriers propagate in the opposite directions, the Hall electrical conductivity σ_{xy} is always positive because of $\nu_e > \nu_h$. However, due to the counter-propagating electron- and hole-like carriers in graphene, the Hall thermal conductivity κ_{xy} can be negative. In order to see the negative κ_{xy} clearly, we show the thermal-gradient-induced terminal bias V_n as well as terminal temperature T_n versus E_0 in Fig. 3. When a temperature difference ΔT is added between the longitudinal terminals 1 and 4, it can induce both temperature difference and also electrical bias between the transverse terminals. In order to satisfy the boundary conditions $I_n = 0$, the bias V_2 (V_3) needs to be higher than the bias V_6 (V_5) [see Fig. 3(a)], which is the Nernst effect (a transverse voltage generated by a longitudinal thermal current).[6–8] As a consequence of $V_2 > V_6$ ($V_3 > V_5$) and the counter-propagating hole-like carriers with the energy $E < E_0$, the temperature T_2 (T_3) has to be lower

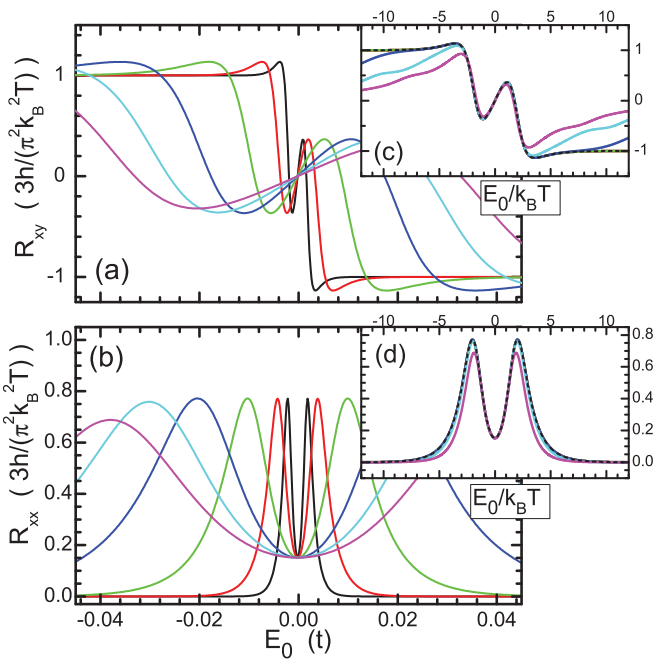

FIG. 2. (Color online) (a) and (b) are, respectively, the magnifications of Figs. 1(b) and 1(c) around the origin $E_0 = 0$. (c) is the result of (a) after scaling using k_BT as dimensionless parameter (i.e., R_{xy} vs E_0/k_BT), while (d) is the same scaling result of (b). The parameters and legend are the same as in Fig. 1. The dotted curves in (c) and (b) are the scaling functions.

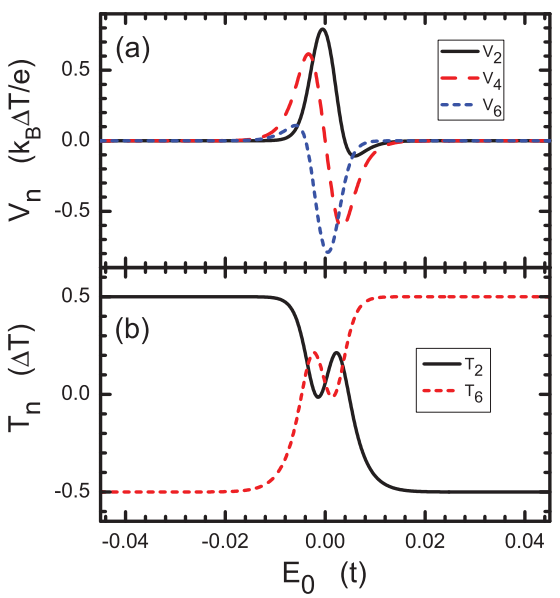

FIG. 3. (Color online) (a) shows the thermal-gradient-induced terminal bias V_n vs Dirac-point energy E_0, while (b) is the terminal temperature T_n as a function of E_0. $k_BT = 0.002t$ and other parameters are the same as in Fig. 1.

than T_6 (T_5) [see Fig. 3(b)] to keep the zero thermal current in all transverse terminals leading to the negative Hall thermal conductivity κ_{xy} and negative Hall-Lorentz number. For the $E_0 > 0$ case, on the other hand, situation of κ_{xy} reverses due to the symmetry of R_{xy}, but the Hall-Lorentz number remains negative in the vicinity of 0.

Next, we study the scaling of fine structure of R_{xy} and R_{xx}. The results are shown in Figs. 2(c) and 2(d). After renormalization of $R_{xy}(R_{xx})$ by using k_BT as a dimensionless unit, all curves (i.e., $R_{xy}(R_{xx})$ vs E_0/k_BT) almost collapse together. In particular, at low T the thermal resistance scales perfectly, while it deviates the scaling law at large $|E_0|$ in the high T case [see Figs. 2(c) and 2(d)]. The general scaling functions can be analytically obtained as follows. When E_F is near the Dirac point at low temperature, T_{nm} can well approximately be $T_{12}(E) = T_{23}(E) = T_{34}(E) = T_{45}(E) = T_{56}(E) = T_{61}(E) = 2\theta(E - E_0), T_{21}(E) = T_{32}(E) = T_{43}(E) = T_{54}(E) = T_{65}(E) = T_{16}(E) = 2\theta(E_0 - E)$, and others are zero. This is because for $E > E_0$ and $E < E_0$ the carriers are, respectively, electron- and hole-like which moves in the clockwise and anti-clockwise direction. Here, the factor 2 is the spin degeneracy. Then, by substituting these transmission coefficients T_{nm} and Eq. (2) into Eqs. (1) and (3), one can straightforwardly obtain the scaling functions as

$$\tilde{R}_{xx}(E_0/k_BT) = 3\{9F_1^4 + (1 - 3F_0 + 3F_0^2)F_2(3F_2 - \pi^2) + F_1^2[9(1 - 2F_0)F_2 + (-2 + 3F_0)\pi^2]\}/A, \quad (4)$$

$$\tilde{R}_{xy}(E_0/k_BT) = \pi^2\{9(-1 + 2F_0)F_1^2 + (1 - 3F_0 + 3F_0^2)(-6F_2 + \pi^2)\}/A, \quad (5)$$

in which $A = -81F_1^4 + 9F_1^2[9(2F_0 - 1)F_2 + (1 - 3F_0)\pi^2] - (1 - 3F_0 + 3F_0^2)(27F_2^2 - 9F_2\pi^2 + \pi^4)$, $F_i \equiv F_i(E_0/k_BT)$, and $F_i(x) = \int_x^\infty x^i/[(e^x + 1)(e^{-x} + 1)]dx, (i = 0,1,2)$. Here, both $\tilde{R}_{xx}$ and $\tilde{R}_{xy}$ are dimensionless, i.e., in the unit of $3h/\pi^2k_B^2T$. By using such scaling functions, many features can be obtained quantitatively. For instance, the maximum value of $R_{xx}(\approx 0.77187)$ lies at $E_0/k_BT \approx \pm 0.23462$, and at $E_0 = 0$, it is $R_{xx} \approx 0.15108$. The minimum value of R_{xy} on the side $E_0 < 0$ is about -0.36709 located at $E_0/k_BT \approx -1.0817$.

Here, we wish to emphasize that, due to the presence of strong magnetic field, the carriers move only along the boundaries of sample, so that our results are independent of the orientation of the edges of the graphene ribbon. As an example, in Fig. 4, we show the Hall thermal resistance R_{xy} for the armchair edge case [see the device schematically shown in Fig. 4(a)]. R_{xy}, in this case, also exhibits the Hall plateaus and the fine structure [see Figs. 4(b) and 4(c)]. For comparison, the results of zigzag edge case are also shown in Figs. 4(b) and 4(c). Now it can be clearly seen that the curves collapse perfectly, including both the Hall plateaus and the fine structure.

In Fig. 5, we examine the influence of magnetic fields ϕ on the Hall thermal resistance R_{xy}. At zero magnetic field ($\phi = 0$), we have $R_{xy} = 0$ everywhere since there is no edge state. With the increase of ϕ from 0, R_{xy} first emerges in the vicinity of $E_0 = 0$ and then it gradually spreads to the whole region. For the small ϕ, only THE (no QTHE) can be observed as seen in

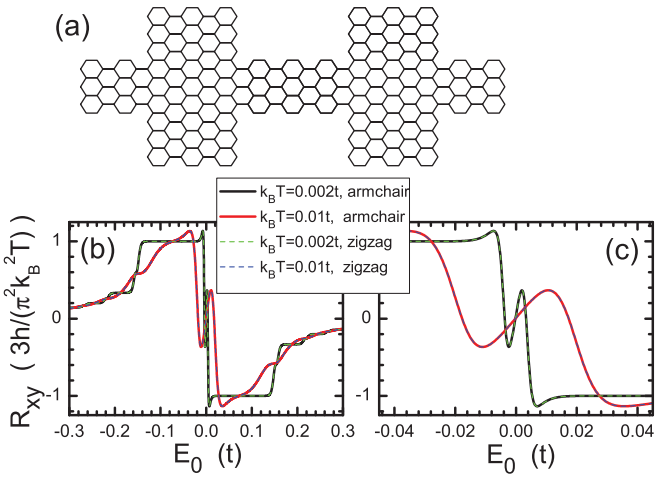

FIG. 4. (Color online) (a) is the schematic diagram for the six-terminal armchair edge graphene ribbon device. In such a schematic diagram, the size is $N = 3$ and $L = 3$. (b) shows R_{xy} for both armchair edge and zigzag edge cases together and (c) is its magnification around the origin $E_0 = 0$. For the armchair edge case, the parameters are $N = 70$, $L = 50$, $\phi = 0.007$, and for the zigzag edge case they are the same as in Fig. 1(b).

Fig. 5(a). But for the large ϕ, Hall plateaus occur due to the formation of Landau levels and edge states. Figure 5(b) shows R_{xy} versus the magnetic field ϕ, in which similar behaviors are observed. In another word, we have $R_{xy} \propto \phi$ at small ϕ, and the plateaus of R_{xy} finally occur at the half-integer values when ϕ is large enough.

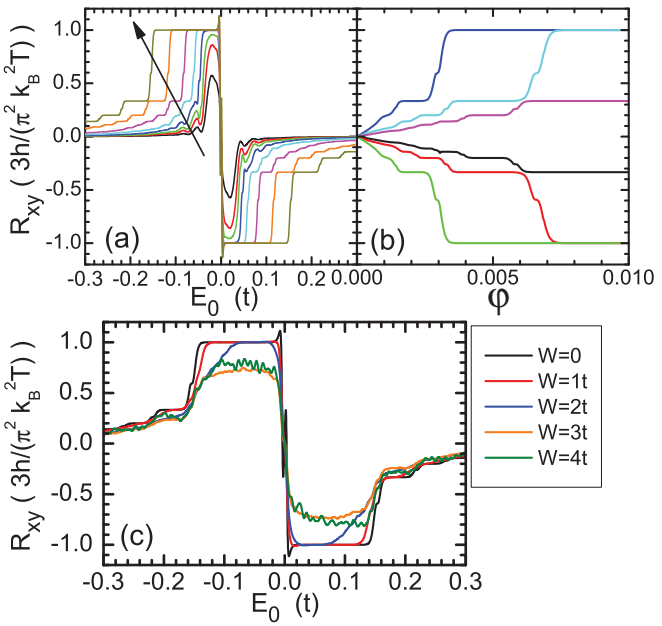

FIG. 5. (Color online) (a) shows R_{xy} vs E_0 for $\phi = 0.0001$, 0.0002, 0.0003, 0.0005, 0.001, 0.002, 0.004, and 0.007 (along the arrow direction), while (b) is R_{xy} vs ϕ for $E_0 = -0.1t$, $-0.15t$, $-0.2t$, $0.2t$, $0.15t$, and $0.1t$ from bottom to top. The parameters are $k_BT = 0.001t$, $N = 50$, and $L = 50$. (c) is R_{xy} vs E_0 at different disorder strengths W with the parameters being $N = 40$, $L = 40$, $\phi = 0.007$, and $k_BT = 0.002t$.

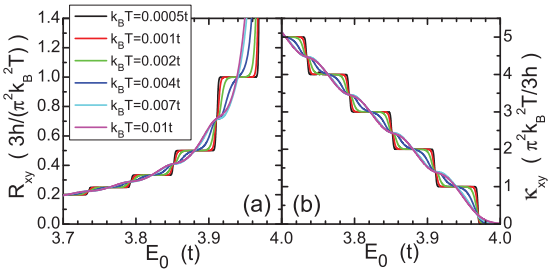

FIG. 6. (Color online) R_{xy} (a) and κ_{xy} (b) vs energy E_0 at different temperatures for the square lattice system. The parameters are $N = 80$, $L = 80$, and $\phi = 0.03$.

Next, we shall examine the disorder effect on R_{xy}. Here, the disorder is assumed to exist only in the central region [see the dotted box in the inset of Fig. 1(d)]. In the presence of disorder, the on-site energy E_0 at site i in the central region becomes $E_0 + w_i$, where w_i is uniformly distributed in the range $[-W/2,\ W/2]$ with W being the disorder strength. In Fig. 5(c), we present the influence of disorder on R_{xy} at different disorder strengths W, from which the results clearly show that, the quantized plateaus of R_{xy} are very robust against disorder effect owing to the topological feature of system. In particular, the lowest plateau $3h/(\pi^2 k_B^2 T)$ remains intact even when the disorder strength reaches up to $W = 2t$, and its fluctuation is nearly 0. When W increases further the plateaus start to deteriorate, but the values of R_{xy} do not decrease very much. In other words, although QTHE is completely destroyed due to the large disorder, the THE still exists. This is due to the following reason. Although the disorder strongly reduces the Hall temperature difference $T_2 - T_6$, the longitudinal thermal current Q is also strongly weakened at the same time, giving rise to a finite value of THE even at $W \to \infty$. On the other hand, the fine structure of R_{xy} with the negative Hall-Lorentz number L_{xy} in the vicinity of $E_0 = 0$ is sensitive to the disorder, and it will be weakened as well. In particular, at a certain disorder strength W, R_{xy} and L_{xy} can change sign, and accordingly the WF law gradually recovers again. In this case, the carriers behave much more like classical carriers due to the strong scattering as a result of disorders.

Finally, for comparison, R_{xy} and κ_{xy} in a usual 2DEG (square lattice) instead of the graphene system (hexagonal lattice) are shown in Fig. 6. Similarly, R_{xy} and κ_{xy} also have quantized plateaus at low temperature, and they become gradually destroyed with the increase of $k_B T$. On the other hand, two main differences are observed. First, the Hall plateaus are at integer values rather than half integers. Second, no fine structure occurs and L_{xy} always remains positive.[13]

IV. CONCLUSION

In summary, the QTHE in graphene system is theoretically investigated. The quantized thermal Hall plateaus at the half-integer values are exhibited at low temperature and they are robust against disorders. Besides, a fine structure with a negative Hall-Lorentz number is found when Fermi energy is near the Dirac point. Finally, all results are insensitive to the orientation of edge and also size of the graphene.

ACKNOWLEDGMENTS

This work was financially supported by NSF-China under Grants No. 10821403, 10974236, and 11074174.

*sunqf@iphy.ac.cn

[1] K. v. Klitzing, G. Dorda, and M. Pepper, Phys. Rev. Lett. **45**, 494 (1980); D. R. Yennie, Rev. Mod. Phys. **59**, 781 (1987).

[2] J. E. Hirsch, Phys. Rev. Lett. **83**, 1834 (1999); S. Murakami, N. Nagaosa, and S.-C. Zhang, Science **301**, 1348 (2003); J. Sinova, D. Culcer, Q. Niu, N. A. Sinitsyn, T. Jungwirth, and A. H. MacDonald, Phys. Rev. Lett. **92**, 126603 (2004).

[3] N. Nagaosa, J. Sinova, S. Onoda, A. H. MacDonald, and N. P. Ong, Rev. Mod. Phys. **82**, 1539 (2010).

[4] M. König, H. Buhmann, L. W. Molenkamp, T. Hughes, C.-X. Liu, X.-L. Qi, and S.-C. Zhang, J. Phys. Soc. Jpn. **77**, 031007 (2008).

[5] C. W. J. Beenakker and A. A. M. Staring, Phys. Rev. B **46**, 9667 (1992).

[6] S.-G. Cheng, Y. Xing, Q.-F. Sun, and X. C. Xie, Phys. Rev. B **78**, 045302 (2008); Y. Xing, Q.-F. Sun, and J. Wang, *ibid.* **80**, 235411 (2009).

[7] O. Cyr-Choinière, R. Daou, F. Laliberté, D. LeBoeuf, N. Doiron-Leyraud, J. Chang, J.-Q. Yan, J.-G. Cheng, J.-S. Zhou, J. B. Goodenough, S. Pyon, T. Takayama, H. Takagi, Y. Tanaka, and L. Taillefer, Nature **458**, 743 (2009).

[8] Z. W. Zhu, H. Yang, B. Fauqué, Y. Kopelevich, and K. Behnia, Nat. Phys. **6**, 26 (2010).

[9] W.-L. Lee, S. Watauchi, V. L. Miller, R. J. Cava, and N. P. Ong, Phys. Rev. Lett. **93**, 226601 (2004); A. Banerjee, Benoit Fauqué, K. Izawa, A. Miyake, I. Sheikin, J. Flouquet, B. Lenoir, and K. Behnia, Phys. Rev. B **78**, 161103(R) (2008); N. Hanasaki, K. Sano, Y. Onose, T. Ohtsuka, S. Iguchi, I. Kézsmárki, S. Miyasaka, S. Onoda, N. Nagaosa, and Y. Tokura, Phys. Rev. Lett. **100**, 106601 (2008); K. Behnia, L. Balicas, and Y. Kopelevich, Science **317**, 1729 (2007).

[10] K. Uchida, S. Takahashi, K. Harii, J. Ieda, W. Koshibae, K. Ando, S. Maekawa, and E. Saitoh, Nature **455**, 778 (2008); Nat. Mater. **9**, 894 (2010); C. M. Jaworski, J. Yang, S. Mack, D. D. Awschalom, J. P. Heremans, and R. C. Myers, *ibid.* **9**, 898 (2010).

[11] K. S. Novoselov, A. K. Geim, S. V. Morozov, D. Jiang, Y. Zhang, S. V. Dubonos, I. V. Grigorieva, and A. A. Firsov, Science **306**, 666 (2004); Nature (London) **438**, 197 (2005); Nat. Phys. **2**, 177 (2006); Y. Zhang, Y.-W. Tan, H. L. Stormer, and P. Kim, Nature (London) **438**, 201 (2005).

[12] C. W. J. Beenakker, Rev. Mod. Phys. **80**, 1337 (2008); A. H. Castro Neto, F. Guinea, N. M. R. Peres, K. S. Novoselov, and A. K. Geim, *ibid.* **81**, 109 (2009); N. M. R. Peres, *ibid.* **82**, 2673 (2010).

[13] H. Oji, Phys. Rev. B **29**, 3148 (1984); Y. M. Blanter, D. V. Livanov, and M. O. Rodin, J. Phys. Condens. Matter **6**, 1739 (1994).

[14] C. L. Kane and M. P. A. Fisher, Phys. Rev. B **55**, 15832 (1997).

[15]K. Krishana, J. M. Harris, and N. P. Ong, Phys. Rev. Lett. **75**, 3529 (1995); Y. Zhang, N. P. Ong, Z. A. Xu, K. Krishana, R. Gagnon, and L. Taillefer, *ibid.* **84**, 2219 (2000); M.-R. Li, Phys. Rev. B **65**, 184515 (2002); A. Vishwanath, *ibid.* **66**, 064504 (2002).

[16]Y. Shiomi, Y. Onose, and Y. Tokura, Phys. Rev. B **79**, 100404(R) (2009).

[17]N. M. R. Peres, J. M. B. L. dos Santos, and T. Stauber, Phys. Rev. B **76**, 073412 (2007).

[18]W. Long, Q.-F. Sun, and J. Wang, Phys. Rev. Lett. **101**, 166806 (2008).

[19]Q.-F. Sun and X. C. Xie, Phys. Rev. Lett. **104**, 066805 (2010).

[20]L. G. C. Rego and G. Kirczenow, Phys. Rev. Lett. **81**, 232 (1998).

[21]Y. Meir and N. S. Wingreen, Phys. Rev. Lett. **68**, 2512 (1992); *Electronic Transport in Mesoscopic Systems*, edited by S. Datta (Cambridge University Press, Cambridge, England, 1995).